Efforts at effective seismic reservoir characterization of Bone Spring and Wolfcamp formations in the Delaware Basin – a case study

Satinder Chopra[†][*], Ritesh Kumar Sharma[†] and James Keay[+]

[†] *TGS, Calgary;* [+]*TGS, Houston*

Summary

The Delaware and Midland Basins are multistacked plays with production being drawn from different zones. Of the various prospective zones in the Delaware Basin, the Bone Spring and Wolfcamp formations are the most productive and thus are the most-drilled zones. A 3D seismic survey was acquired in the northern part of Delaware Basin and after processing was picked up, to understand the reservoirs of interest and pick the sweet spots. We describe the whole reservoir characterization exercise that was carried out on this data in three different phases. We discuss phase 1 here, beginning with a brief description of the geology of the area and the stratigraphic column, and going on to the well ties for the different available wells over the 3D seismic survey, estimation of the shear curves where the measured shear curves were missing, the generation of an accurate low-frequency model for impedance inversion, preconditioning of the prestack seismic data, use of different lithotrends in inversion and finally the prestack simultaneous impedance inversion.

Introduction

The Permian Basin in west Texas and southeast New Mexico is the most prolific of all the basins in the US. The Delaware Basin forms the western subbasin of the Permian, the Midland Basin the eastern part, and both are separated by the Central Basin Platform (Figure 1). The Delaware and Midland Basins are multistacked plays with production being drawn from different zones. Of the various prospective zones in the Delaware Basin, the Bone Spring and Wolfcamp formations are the most prolific and thus the most-drilled zones.

3D seismic data acquisition and processing

A three-dimensional seismic survey was acquired in the Delaware Basin, spread over the Ward, Loving and Winkler counties (Figure 1). The size of the seismic survey was 407 mi^2 (1050 km^2) and its acquisition completed in November 2017. The seismic data had 2 ms sample interval, 5 s record length, and with a bin size of 82.5 ft. by 82.5 ft. (25.2 x 25.2 m). The processing of this large data volume was completed in May 2018 with anisotropic prestack time migration (PSTM) gathers and stacked volume with 5D interpolation. The processing of the data was completed in April 2018 and picked up with the *objective of seismic reservoir characterization that would help in understanding the reservoirs of interest and prove useful towards cost-effective drilling*.

Targets formations of interest

The formations of interest in the Delaware Basin are the Bone Spring, Wolfcamp, Barnett and the Mississippian. We focus on the first two in this study. The thickness of the Bone Spring Formation varies from 700 m to 1000 m, which was deposited in three different cycles, separated by carbonate sequences. While the sands were deposited as turbidities during low sea levels, the black bituminous-rich limestones were deposited in deep euxinic basinal environments. These units, in particular the Avalon shale, may contribute as source rocks in the Delaware Basin. During the

Wolfcampian, dark shale and limestone with silt and sand zones characterize the central parts of the basin and carbonate buildups and banks on the shelf areas.

With the above geologic information in mind, a deep well (W11) was selected over the 3D seismic volume (location indicated in Figure 1), and the well curves were correlated with the seismic data. The different lithounits were identified on the log curves with the available formations tops and the equivalent intervals were identified on the seismic data. We found that while the Mississippian, Bone Spring and Bell Canyon were found to be trackable on the seismic data, other horizons such as Wolfcamp (along with its subunits), and Barnett were not easily trackable. The broad zone of interest extends from the Bell Canyon (close to 800 ms) to Mississippian (close to 2800 ms), an overall interval of 2 seconds. The two main lithounits of interest, i.e. the Bone Spring and the Wolfcamp zones and their subunits, i.e. the 1st, 2nd and 3rd Bone Spring sands and carbonates as well as Wolfcamp (A, B and C) are indicated on the lithocolumn (Figure 2).

Well-to-seismic ties

In a large time-window of interest, a single wavelet would result in reflection event mismatch, and in flawed formation calibration as well. If such a wavelet is utilized for performing seismic impedance inversion, it could possibly result in missing geologic features or subsequently result in inaccurate estimation of rock properties. In the present exercise, as the time window spanning Bone Spring to Mississippian is over 2 seconds long, *the idea of extraction of a single average seismic wavelet over that window was not considered advisable, and so was abandoned*. Besides, on examining the wavelets extracted in overlapping time windows and their frequency spectra at four different well locations on the 3D seismic volume, it was found that for the wells to the right side of the survey, due to their proximity to the Central Basin Platform, the wavelet shapes and their frequency spectra were somewhat different from their counterparts to the left. Thus, we decided to not only go for time-variant extraction of wavelets in overlapping time windows, but also to consider the spatial variation of the wavelet character in our analysis, especially impedance inversion.

Low-frequency model building for impedance inversion

For the generation of an interval velocity field using well-log data, the usual practice is to low-pass filter (<10 Hz) the available sonic well-log curves and use one or more of the derived curves for generation of the interval velocity field using extrapolation or interpolation and guided by horizon boundaries. Where more than one well is used for the generation of the interval velocity field, usually an inverse-distance weighted scheme or a process called *kriging* is utilized. Such techniques should be used with care as they can produce artifacts in the form of artificial tongues of sharp velocity changes that are nongeologic.

Instead of using such a technique that could be fraught with problems, we instead make use of a relatively new approach for the generation of an interval velocity field that utilizes both well-

log data and seismic data to establish the relationship between seismic attributes and the well-log curves. In this approach the low frequency velocity model generated with a single well is used as one of the inputs, and some other seismic attribute data volumes, a multiregression approach (Ray and Chopra, 2016) is used, wherein a target interval velocity log is modeled as a linear combination of several input attributes at each sample point. In the case at hand, we extended this approach to including two wells (W3 and W7) to capture the varying geological trend from east to west. We determine the correct number of attributes to use by what is referred to as a crossvalidation method (Hampson et al., 2001).

Estimation of shear curves

Shear-wave velocity is measured directly in the borehole with a dipole shear tool but is usually not available in all the wells used for analysis in a project. The reasons for nonavailability of the shear log curves in wells vary from the old wells not having them to the cost associated with their acquisition. In the interest of economics again, many oil companies do not continuously record shear log curves over the length of the wells where the sonic or other curves may be acquired. Consequently, shear curves are commonly recorded over short intervals in wells.

Different workers have suggested the use of empirical (Castagna et al., 1985; Greenburg and Castagna, 1992) or theoretical (Krief et al., 1990) relationships for estimation of shear velocity from the available compressional velocity information. Such computations were initially suggested for sandstones, which may or may not be generalized for every subsurface formation. Also, recognizing the fact that the relationships between compressional and shear velocity may not be a straightforward linear one, other workers have demonstrated the use of artificial neural networks for shear velocity well-log estimation by making use of other well curves. Generally, it is found that better correlations exist between the neural network-estimated shear curves with the measured shear curves used as blind wells, than a simple application of an empirical relationship.

For the 3D dataset at hand, 3 wells (W4, W12 and W9 in Figure 1) were available with shear curves in addition to sonic, gamma ray, resistivity and porosity, over an interval from Bell Canyon to Mid-Wolfcamp. The neural networks were trained on these wells followed by crossvalidation analysis. Thereafter, shear curves were predicted for the wells W13 and W2, which were not used in the training of the neural networks. While well W13 had measured shear curve from Bell Canyon to Mid-Wolfcamp, well W2 had this curve for Mid-Wolfcamp to Barnett.

A good correlation was found between the neural network-estimated shear velocity and that measured in the two blind wells. In the present study, the impedance inversion is to be carried out from Bone Spring to Mississippian, and as shear curves are not available over such large intervals, confidence in the estimated shear curves over Bell Canyon to Mid-Wolfcamp and from this level to Barnett helped us proceed with the estimation of shear curves for all the deep wells that had sonic and density curves. A crossplot of P- and S-impedance was generated for all the deep wells, wherefrom a linear relationship was determined, which was then used to generate the shear wave low frequency impedance model for simultaneous impedance inversion. Besides this important application, the estimation of shear information as discussed above forms a very crucial role in lithologic trend analysis as is discussed later.

Preconditioning of seismic data

The seismic data were conditioned carefully to make sure that amplitudes are preserved such that their variation with offset/angle could be utilized in a meaningful way. The major processes employed in the conditioning were supergathering (3x3), bandpass filtering, random-noise attenuation and trim statics, with difference plots taken at each step to ensure that no useful signal was distorted or attenuated.

As an important QC during preconditioning of prestack seismic data we plotted amplitudes as a function of offset before and after preconditioning at selected events at each prominent processing step and noticed that the scatter of amplitude values after preconditioning is reduced, but the overall gradient remains the same.

Offset-to-angle transformation

While seismic data are acquired and processed in offset domain, AVO analysis or simultaneous inversion are performed in the angle domain. Usually for the transformation of offsets into angles, the relationship given by Walden (1991) is utilized. Two types of velocities, namely seismic and well velocity are available for analysis. During processing of seismic data, the velocity analysis yields the RMS velocity field, which can then be converted into an interval velocity field using Dix's (1955) hyperbolic approximation relationship. Usually, seismic velocity has its own limitations due to limited resolution and not necessarily being horizon-consistent.

As well velocity is considered as the ground truth measurement, it is tempting to use it for domain conversion. However, it needs to be decided whether a single well would be sufficient to represent the whole 3D seismic volume or more wells need to be considered in the analysis.

As we began analyzing the available well-log data, we came across an interesting observation. On the crossplots of P-velocity and gamma ray there were distinct differences in cluster density of points, for wells to the western and eastern side of the survey. Figure 3 shows a crossplot between P-velocity and gamma ray for a pair of wells to the north, namely W1 and W8. The time window for the points crossplotted is Bone Spring to Top Wolfcamp. The cluster points in red come from well W1 and those in green from well W8. Notice the pronounced separate clustering of the red and green points on the crossplot. Similar observations were made for the two other pairs of wells and examined. These crossplots suggest significant differences in velocity and gamma ray between the wells on the western and eastern side of the survey.

Hence multiple wells should be considered in the velocity model building process. But, as mentioned earlier, the use of multiple wells brings its own problems in the analysis and need to be used carefully. *Therefore, we followed the multiregression approach as discussed earlier.* We thus generated the angle of incidence values at each gather using the seismic interval velocity field and the well interval-velocity field and compared them by overlaying them on the seismic offset gathers as shown in Figure 4.

An interesting observation may be made here. As the seismic velocity picking is done by following an increasing trend with time, *even in the presence of a sharp contrasting interface in the subsurface, the angle of incidence does not exhibit any appropriate change there.* Notice at the level of the Mississippian marker and a couple of other locations in the middle, there is no change in the angle of incidence with seismic velocities, while the

2

changes in the computed angle of incidence using well data are changes seen at the different points as expected. Due to this convincing observation, we went along with angle-of-incidence computation using well-log data.

Prestack simultaneous impedance inversion

In simultaneous prestack inversion, multiple partial-offset or angle substacks are inverted simultaneously. For each angle stack, a unique wavelet is estimated. Subsurface low-frequency models for P-impedance, S-impedance and density constrained with appropriate horizons in the broad zone of interest, are constructed using the approach explained above. The models, wavelets and partial stacks were used as input in the inversion, and the output was P-impedance, S-impedance and density. The mathematical formulation for the present implementation of prestack simultaneous impedance is described in Hampson et al. (2005).

Quality control of data going into simultaneous impedance inversion

(a) Dealing with noisy near-angle stack data

Once the angle gathers were generated for the seismic volume, the different angle sub-stacks were generated. On examination, the near-angle stack (1-9°) was found to be noisier than the other angle stacks, e.g. (9 to 18°), and (18 to 27°). When noisier near angle stacks are used in the impedance inversion, the computed P- and S-impedance data are found to have low signal-to-noise ratio. To avoid this, we weighed in on a couple of options, such as leaving out the near-angle stack, or replacing it with the intercept stack computed using a two-term Aki-Richard equation. In Figure 5 we show a comparison of segments of sections from the near angle stack with the intercept stack, where the latter shows a higher signal-to-noise ratio. We went ahead with computing the P-impedance in each of these cases, and on analyzing the results decided to replace the near angle stack with the intercept stack in the simultaneous inversion.

(b) Dealing with different lithological trends in the zones of interest

Realizing that the zones of our interest in 3D seismic data at hand span through the Bone-Spring, Wolfcamp, Barnett shale and Mississippian formations, a key question to answer is which back ground trend should be considered in the inversion. Would a single trend be adequate for defining the background trend? In a thin zone picked up for impedance inversion where a reservoir does not have facies complications, the above suggestion may be good. However, facies complications exist in the area of study and different facies may have different background trends. Thus, it may not be appropriate to use only a single background trend in the impedance inversion. To deal with such a scenario the following approach was followed.

We began with crossplotting of P-impedance, S-impedance and density using available well-log data over the formations of our interest, and search for existing trends in the crossplot space for optimization of the inversion. We believe that the above approach is a better way of handling the facies complication problem *rather than following an approach that starts with different facies trends in the low-frequency domain*. The problem associated with the latter approach is that for defining the different facies before running the inversion, *a calibrated petrophysical model is required*, which most of the time is not available.

Following our approach, in Figure 6 a to d, we exhibit crossplots between $\ln(I_P)$ and $\ln(I_S)$ as well as between $\ln(I_P)$ and $\ln(\rho)$ for individual intervals comprising (a) the overall zone from Bell Canyon to the Mississippian, (b) Bone Spring to Top Wolfcamp, (c) Bell Canyon to Bone Spring, and (d) Top Wolfcamp to Mississippian. If such a crossplot is constructed for the overall zone (Bell Canyon to Mississippian), four different trends can be drawn through the cluster points, suggesting a separate trend for each of the intervals of interest. This significant observation prompted us to not carry out simultaneous inversion in a large time window using a single average rock physics or facies trend. We therefore decided to carry out simultaneous impedance inversion in individual lithounits, comprising Bone Spring to Top Wolfcamp, Top Wolfcamp to Mississippian, …. and merge these impedance intervals into a composite volume.

In Figure 7, we show a comparison of segments of an arbitrary line passing through two wells (W14 and W6) drawn from the P-impedance volume generated using a single trend and then different litho-trends in the complete zone. Notice the difference between them as indicated with coloured arrows. Similar comparisons were carried out for the sections drawn from the S-impedance and V_P/V_S data volumes and valid differences were noticed.

(c) Spatial variation of wavelets

Earlier, we have seen significant differences between the crossplots generated between P-velocity and gamma ray for pairs of wells, one to the west and the other to the east. Also, on examining the different angle stacks we found spatial changes in the reflection detail in that to the east higher amplitude reflections are observed, whereas to the west, the reflections exhibit low amplitudes. Similarly, as stated earlier, the extracted wavelets in the wells to the east and west show variations. All these observations are suggestive of the fact that there would be spatial variations in the seismic wavelets. We therefore decided to account for this spatial variation in the simultaneous impedance inversion as well as the rock physics attributes derived therefrom. Wavelets were extracted at the different wells and interpolated in between them using the available commercial software package.

Conclusions

Our endeavor in this whole exercise has been to bring in accuracy in the different zones constituting the rather large lithounits from Bone Spring to Mississippian. For this we have *paid attention to considerations such as accounting for the temporal and spatial variation of the wavelets embedded in the seismic data, generating an accurate low-frequency model, and employing different facies trends in the individual inversion windows*. We firmly believe that all these considerations have added interpretation value to the products that we have generated so far and used them for generating different characterization elements such as rock physics analysis, determination of faults and fracture analysis and lithofacies classification which are being discussed in other presentations.
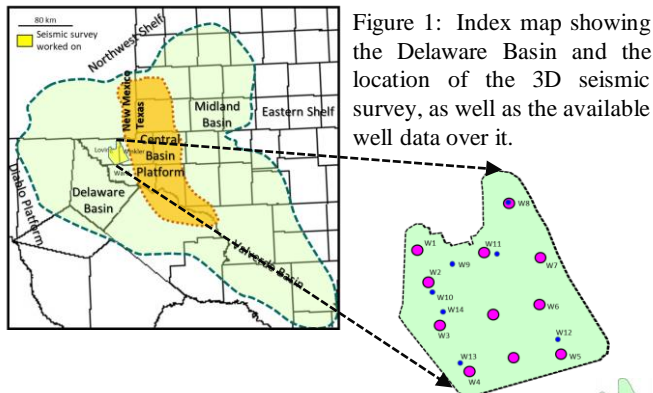
Acknowledgements

3

Figure 1: Index map showing the Delaware Basin and the location of the 3D seismic survey, as well as the available well data over it.
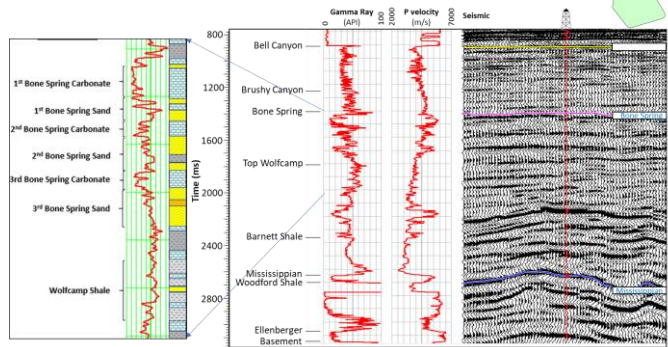
Figure 2: Correlation of well curves for a deep well on the 3D seismic data volume. The litho-column for the Bone Spring and Wolfcamp intervals is shown to the left. *(Data courtesy: TGS, Houston)*
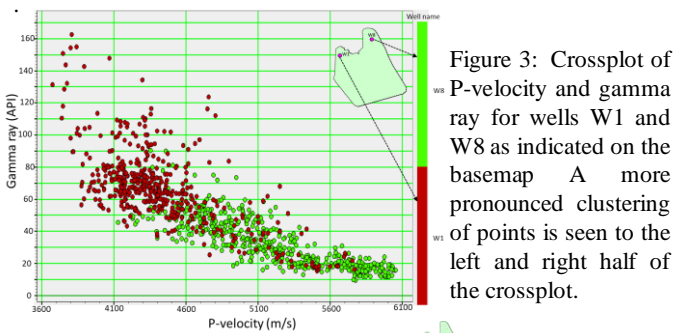
Figure 3: Crossplot of P-velocity and gamma ray for wells W1 and W8 as indicated on the basemap A more pronounced clustering of points is seen to the left and right half of the crossplot.
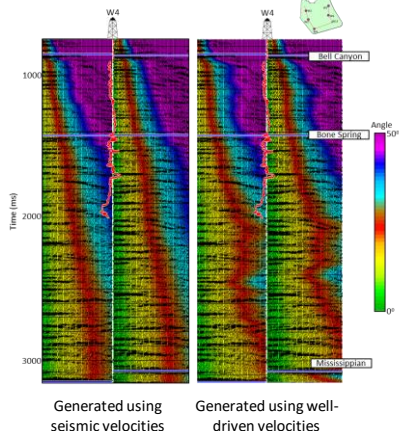
Figure 4: The angles of incidence computed using the seismic interval velocities (left) and well-driven velocities (right) overlaid on seismic offset gathers. The sonic velocity curves have been overlaid at the well location. Notice that while the seismic velocities show an increasing trend, there are sharp changes in the angle of incidence at different points in time as seen on the display for angles of incidence generated using well data.*(Data courtesy: TGS, Houston)*
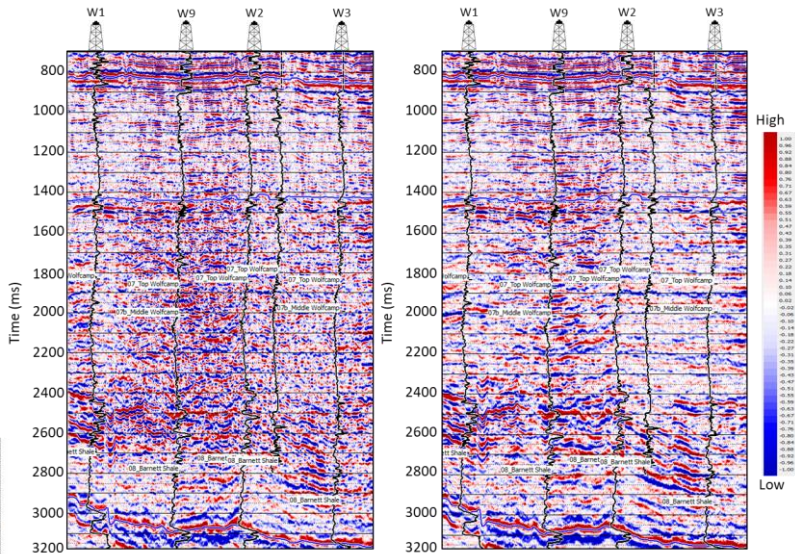
Figure 5: An arbitrary line passing through the (left) near-angle stack, and (right) intercept volume. . *(Data courtesy: TGS, Houston)*
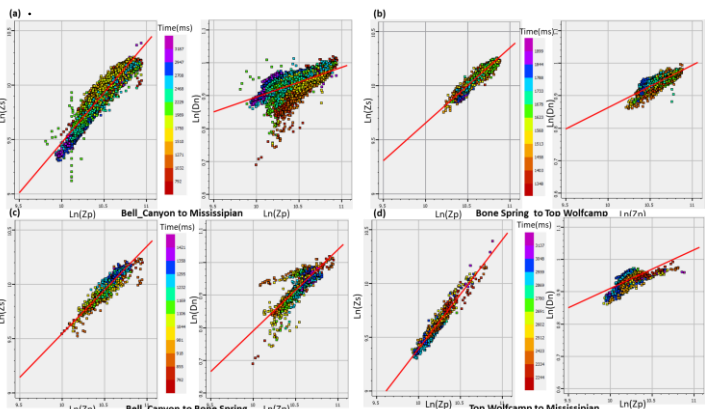
Figure 6: Lithological trend analysis in terms of crossplots to be used in impedance inversion in different litho-intervals, (a) Bell Canyon to Mississippian, (b) Bone Springs to Top Wolfcamp, (c) Bell Canyon to Bone Spring, and (d) Top Wolfcamp to Mississippian. Notice all these trends are different. *(Data courtesy: TGS, Houston)*
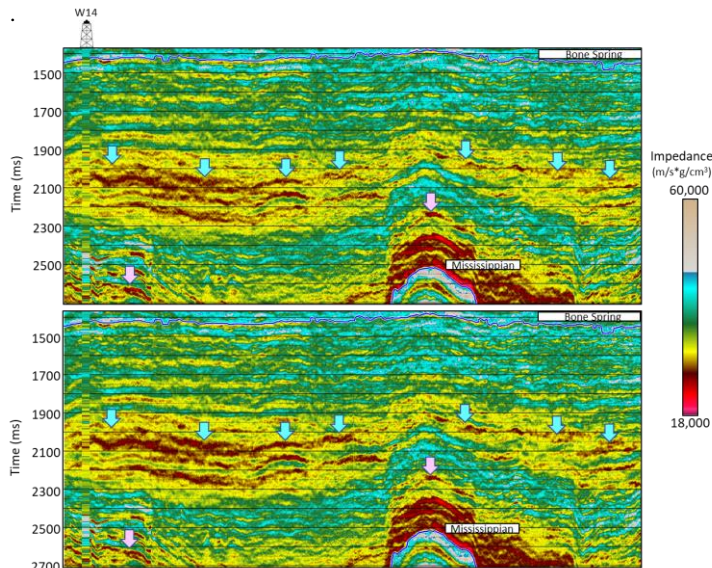
Figure 7: Inverted P-impedance sections along the arbitrary line passing through two wells where same and, (below) different litho-trends are used in the inversion analysis. *(Data courtesy: TGS, Houston)*

REFERENCES

Castagna, J. P., M. L. Batzle, and R. L. Eastwood, 1985, Relationships between compressional-wave and shear-wave velocities in clastic silicate rocks: Geophysics, **50**, no. 4, 571–581, doi: https://doi.org/10.1190/1.1441933.

Dix, C. H., 1955, Seismic velocities from surface measurements: Geophysics, **20**, 68–86, doi: https://doi.org/10.1190/1.1438126.

Greenberg, M. L., and J. P. Castagna, 1992, Shear-wave velocity estimation in porous rocks: Theoretical formulation, preliminary verification and applications: Geophysical Prospecting, **40**, 195–209, doi: https://doi.org/10.1111/j.1365-2478.1992.tb00371.x.

Hampson, D. P., B. H. Russell, and B. Bankhead, 2005, Simultaneous inversion of pre-stack seismic data: 75th Annual International Meeting, SEG, Expanded Abstracts, 1633–1637, doi: https://doi.org/10.1190/1.2148008.

Hampson, D. P., J. S. Schuelke, and J. A. Quirein, 2001, Use of multiattribute transforms to predict log properties from seismic data: Geophysics, **66**, 220–236, doi: https://doi.org/10.1190/1.1444899.

Krief, M., J. Garat, J. Stellingwerff, and J. Ventre, 1990, A petrophysical interpretation using the velocities of P and S waves (full-waveform sonic): The Log Analyst, **31**, 355–369.

Ray, A. K., and S. Chopra, 2016, Building more robust low-frequency models for seismic impedance inversion: First Break, **34**, 47–52, doi: https://doi.org/10.3997/1365-2397.2016005.

Walden, A. T., 1991, Making AVO sections more robust: Geophysical Prospecting, **39**, 915–942, doi: https://doi.org/10.1111/j.1365-2478.1991.tb00350.x.